Quantum Chemical Study on the Coordination Environment of the Catalytic Zinc Ion in Matrix Metalloproteinases

Natalia Díaz,* Dimas Suárez, and Tomás L. Sordo

Departamento de Química Física y Analítica, Universidad de Oviedo C/Julián Clavería 8, 33006 Oviedo (Asturias), Spain

Received: September 1, 2006

X-ray analyses of matrix metalloproteinases (MMPs) have shown that the catalytic zinc ion (Zn1) can bind to one to three water molecules in addition to three conserved histidine residues. To estimate the relative stability of the possible Zn1 coordination structures in the active site of the MMPs, we carry out computational analyses on the coordination environment of the Zn1 ion in the gelatinase A enzyme (or matrix metalloproteinase 2; MMP-2). Four-, five-, and six-coordinated complexes representative of the Zn1 site are fully characterized by means of quantum mechanical (QM) methodologies. On one hand, B3LYP/LACVP* minimizations of various cluster models of the MMP-2 active site show that the trigonal bipyramidal geometry is energetically favored in the gas phase and that continuum solvent effects stabilize preferentially the tetrahedral complexes. On the other hand, B3LYP/OPLS-AA hybrid QM/molecular mechanical calculations in the solvated catalytic domain of the MMP-2 enzyme complemented with electrostatic Poisson−Boltzmann calculations show that the mature enzyme presents most likely a Zn1 ion coordinated by three histidine residues and two water molecules, while the active site glutamic acid is negatively charged. In consonance with X-ray diffraction data, other possible Zn1 configurations, a six-coordinated structure with Zn1−water as well as four- and five-coordinated complexes with a Zn1-bound hydroxide, are predicted to be very close in energy.

Introduction

Matrix metalloproteinases (MMPs) are a family of zinc-dependent endopetidases capable of hydrolyzing virtually all kinds of extracellular matrix proteins.[1,2] This hydrolytic activity plays a central role in all physiological processes requiring tissue turnover and remodeling and contributes to modulate normal cellular behavior and cell−cell communication.[3,4] The MMPs are also associated with a variety of pathological conditions, ranging from cancer[5,6] to arthritis[7,8] and multiple sclerosis, where the aberrant hydrolytic activity performed by these enzymes contributes to the progress of the disease. Thus MMP inhibition is considered a novel therapeutic strategy in the treatment of some of these diseases and is currently an attractive and active trend in structure-based drug design.[9−12]

On the basis of their structure and preferred substrates, the MMP family can be divided into several main classes that include collagenases, gelatinases, stromelysins, membrane-type MMPs, and a more heterogeneous subgroup including matrylysins, metalloeslastase, and so forth.[13] All of them share a significant sequence homology and, in most cases, a common multidomain structure formed by an N-terminal prodomain, a catalytic domain, and a C-terminal hemopexin-like domain.[14−16] The prodomain has a unique and highly conserved cysteine-containing sequence ("cysteine switch") that binds zinc in the catalytic domain of the inactive enzyme. This N-terminal domain (about 80 amino acids) is removed upon activation. The catalytic domain (about 170 residues) that is responsible for the hydrolytic activity consists of a twisted five-stranded β-sheet, three α helices, and several bridging loops. In gelatinases, the catalytic domain has an additional 175 amino acid residue insert comprising three fibronectin-related type II modules conferring gelatine and collagen binding properties. The C-terminal hemopexin-like domain, which is linked to the catalytic domain by a hinge peptide, presents a four-bladed propeller structure and probably plays a role in substrate recognition.

The active site located in the catalytic domain contains a conserved zinc binding motif, HEXXHXXGXXH, responsible for coordinating the catalytic zinc ion (Zn1) by means of three histidines. It also includes a conserved glutamate residue that, according to mutagenesis experiments, is critical for catalysis.[17,18] The catalytic domain of all MMPs contains a second zinc ion (Zn2), the so-called structural zinc, and one to three calcium ions that are likewise supposed to play a structural role.[16] The structural zinc is always liganded in a tetrahedral coordination sphere made up of three histidines and one of the oxygen atoms from an aspartic acid side chain. The calcium ions are octahedrally coordinated by protein residues and water molecules.

In addition to the three conserved histidines of the zinc binding motif, X-ray diffraction studies revealed that the Zn1 ion can coordinate one, two, or three water molecules. To date, only one X-ray structure of a MMP catalytic domain in its active form has been determined, which corresponds to a truncated MMP-3 enzyme (PDB code 1CQR, 2.0 Å).[19] In this structure, one of the protein molecules in the unit cell (chain B) shows a tetrahedral Zn1 ion coordinated to a water molecule which, in turn, interacts with the conserved glutamic acid. Other high-resolution X-ray structures of modified and/or inhibited MMPs show Zn1···water contacts that could be relevant for the active form of the MMPs. Thus, the X-ray structures of three different pyrimidine dicarboxamide inhibitors bound in the S1′ pocket of the MMP-13 enzyme show one or two water molecules in the first coordination shell of Zn1 (PDB codes 1XUR, 1XUD,

* Corresponding author. Phone: +34-985105010. Fax: +34-985103125. E-mail: diazfnatalia@uniovi.es.

10.1021/jp0656882 CCC: $33.50
Published on Web 11/09/2006

SCHEME 1

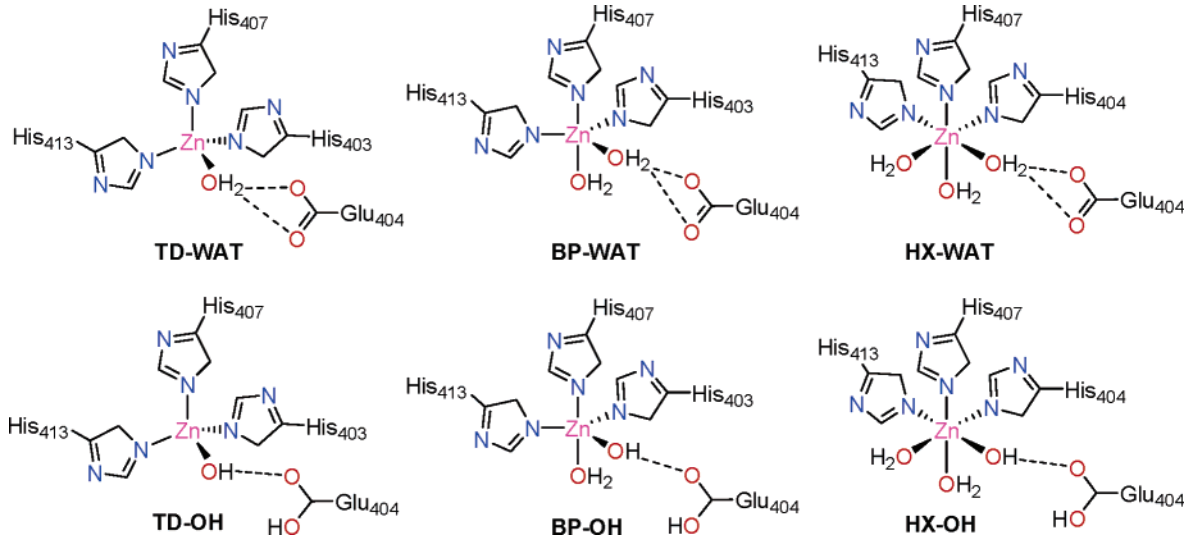

and 1XUC; 1.70−1.85 Å).[20] Similarly, the crystal structure of the F171D mutant of the catalytic domain of MMP-12 has six chains in the unit cell in which the Zn1 ion is coordinated to a variable number (one to three) of water molecules (PDB code 1OS9, 1.85 Å).[21] On the other hand, extended X-ray absorption fine structure (EXAFS) analyses have been performed on the active form of MMP-2 and MMP-9 showing that the catalytic and structural zinc ions have a similar atomic environment.[22,23] These results suggested that water molecule(s) could be bound to the Zn1 ion in the active form of the gelatinases. It must be noted, however, that during the EXAFS curve-fitting analysis only the σ^2 parameter, which provides a measure of thermal and static disorder, and the interatomic metal−ligand distances, *R*, were allowed to float, whereas the average coordination numbers, *N*, were fixed by using the crystallographic coordinates of the pro-MMP-2 enzyme (2.8 Å of resolution) in which the two zinc ions display tetrahedral coordination.

The first coordination shell around Zn1 in the crystal structures of the latent and/or Zn1-inhibited forms of MMP enzymes, which does not include water molecules, is able to accommodate four or five ligands. For the pro-MMPs (i.e., propeptide covalently bound to the MMP catalytic domain), Zn1 has a tetrahedral arrangement with the propeptide cysteine side chain acting as the fourth ligand.[24,25] The natural inhibitors of MMPs (tissue inhibitors of matrix metalloproteinases, TIMPs) bind to Zn1 in a bidentate manner through the amino and carbonyl groups of the cysteine1 backbone resulting in a pentacoordinated metal ion.[26,27] For the MMPs complexed with synthetic inhibitors, various coordination environments around Zn1 have been observed: sulfur- and phosphorus-containing inhibitors interact with Zn1 in a monodentate manner resulting in a tetrahedral geometry, whereas carboxylic acids and hydroxamates serve as bidentate ligands to Zn1 in a distorted trigonal bipyramidal geometry.[9,15,16,21,28]

Clearly, the crystallographic characterizations of Zn1···ligand and Zn1···water interactions in different MMP enzymes suggest that the Zn1 ion possesses a flexible first coordination shell that can adopt various coordination numbers. However, a detailed computational analysis of the geometry and energies of the different coordination modes accessible to the active form of the MMP enzymes has not been performed. Such a computational analysis complements the X-ray structural information and can be considered a prerequisite to the theoretical examination of substrate binding and reaction mechanisms.[29] In this work, we investigated the coordination sphere of the catalytic zinc ion in the active form (i.e., in the absence of inhibitors and pro-peptide) of the catalytic domain of the gelatinase A (MMP-2). This enzyme is a key player in vascular development and angiogenesis whose expression has been demonstrated in many different human tumors.[30] We employed both quantum mechanical (QM) and hybrid quantum mechanical/molecular mechanical (QM/MM) methods. First, we optimized a series of cluster models of the MMP-2 active site considering several coordination environments (four, five, and six) for Zn1 as well as various ionization states for the Zn1-bound water molecules and the essential glutamic acid residue (see Scheme 1). Subsequently, the effect of the whole catalytic domain and solvent was taken into account by means of QM/MM and Poisson−Boltzmann (PB) calculations. Finally, we comment on the ability of the computational results to gain insight into the structure and catalytic activity of the MMP-2 enzyme.

Methods

QM Level of Theory. We employed a density functional theory (DFT) method for stand-alone QM calculations on gas-phase models and for the QM region in the QM/MM calculations on the MMP-2 enzyme. The comparison between the QM/MM results for the enzyme and the QM results for the gas-phase cluster systems will allow us to assess the role of the protein environment on the coordination of the Zn1 ion. For the sake of consistency, the same QM level of theory was employed in the cluster and in the enzyme calculations. In particular, our QM and QM/MM calculations on the MMP-2 models were carried out using the B3LYP functional[31,32] with the double-ζ 6-31G* basis set for nonmetal atoms and the Los Alamos effective core potentials for zinc[33] (this mixed basis set will be denoted as LACVP*). We note that this QM level of theory together with the OPLS force field has been specifically optimized for modeling protein active sites, with parametrization enabling the QM region to be defined via a series of cuts in the backbone and at the side chains between Cα and Cβ atoms.[34]

Validation Calculations. From previous computational experience in metal-containing systems, the error on the relative energies computed by DFT methodologies is unlikely to exceed a range of 3−5 kcal/mol.[35,36] Nevertheless, exceptions exist, and therefore, the performance of the B3LYP/LACVP* level

SCHEME 2

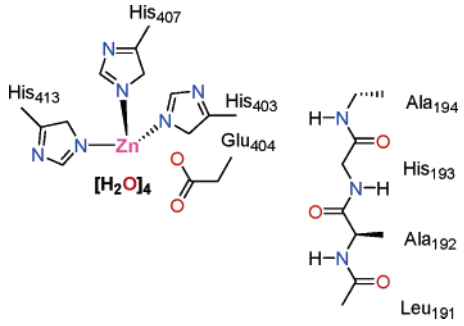

as compared with ab initio methodologies is reassessed in this work. Thus, we performed a series of validation calculations on small zinc compounds that are relevant to the coordination environment of the Zn1 site in the MMP-2 active site. Molecular geometries of the small systems were optimized at the B3LYP/LACVP* and MP2/6-31+G** levels of theory (the full electron 6-31+G** basis set for Zn[37] was used in the MP2 calculations). To estimate the effect of larger basis sets and more elaborate N-electron treatments on the ab initio energies, single-point CCSD(T)/6-31+G** and MP2/6-311+G(3df,2p) calculations were performed on the MP2/6-31+G** geometries. All of the gas-phase validation calculations were carried out with the Gaussian03 program.[38] The effect of the polarity of the environment was estimated by means of single-point B3LYP/LACVP*/HF/6-31+G** self-consistent reaction field (SCRF) calculations on the gas-phase B3LYP/LACVP*/MP2/6-31+G** geometries using the PB solver[39] included in the Jaguar program.[40]

QM Calculations on Cluster Models. The initial coordinates for the cluster atoms were extracted from the 1CK7 crystal structure corresponding to the Ala404Glu mutant of the full-length pro-MMP-2 enzyme (2.8 Å resolution).[24] The cluster models comprised the His_{403}, His_{407}, and His_{413} side chains that coordinate the catalytic zinc ion through their Nϵ atom and the Glu_{404} side chain that was modeled using the coordinates of Ala_{404}. In addition, a fragment of the β4 strand that delimitates the active site (the Cα−CO moiety of Leu_{191}, the Ala_{192} residue, the His_{193} backbone, and the HN−Cα−Cβ moiety of Ala_{194}) was also included (see Scheme 2 and Figure S2 in Supporting Information). Four water molecules were added to the cluster models in order to analyze different coordination numbers of Zn1.

The cluster models corresponding to the active site configurations shown in Scheme 1 were minimized on the B3LYP/LACVP* potential energy surface (PES) using the Jaguar program.[40] During geometry optimizations, the Cβ atom of the residue side chains and the link H atom attached to it (i.e., the H atom that "replaces" the Cα atom) were fixed at their initial positions. For the β4-strand moiety, the carbonyl O atoms as well as the terminal methylene groups were also fixed in order to preserve the orientation observed in the initial crystal structure. Analytical frequency calculations were performed at the B3LYP/LACVP* level using the Gaussian03 program[38] and the converged wave function from Jaguar. The Hessian matrix was then transferred to the Jaguar program in order to characterize the critical points and compute thermodynamic data at 298 K.

Single-point B3LYP/LACVP* SCRF PB calculations[39] were also carried out on the gas-phase QM geometries using Jaguar. Several values for the dielectric constant of the surrounding continuum (ϵ) were considered to analyze the trend in the relative solvation energies: 80 (water, high polarity), 20 (intermediate polarity), and 4 (low polarity). For comparative purposes, solvation energies were recomputed using the Delphi program[41,42] and the charges derived from the B3LYP/LACVP* electrostatic potential (ESP). In the Delphi calculations, the linearized PB equation on a cubic lattice was solved by using an iterative finite-difference method (1000 iterations) and a grid spacing of 0.5 Å. The van der Waals surface was constructed using DREIDING van der Waals radii for C, H, N, O, and Zn atoms. The dielectric boundary was the contact surface between the radii of the solute and the radius (1.4 Å) of a water probe molecule. The Debye−Hückel approximation was used to determine the potentials at the boundary of the grid.

QM/MM Calculations on the MMP-2 Catalytic Domain. Coordinates for the catalytic domain of MMP-2 were extracted from the 1CK7 crystal structure after deleting the propeptide (Pro_{31}-Tyr_{110}) and the C-terminal haemopexin domain.[43] The three fibronectin-type domains present in MMP-2 were replaced by a short peptide segment (Lys-Gly-Val) observed in other X-ray structures of MMP-2.[44] The catalytic and structural zinc ions, two calcium ions, and the crystallographic water molecules near the catalytic domain were preserved. The total number of protein atoms including hydrogens is 2532.

The catalytic domain was solvated by a water cap of 25 Å centered at the Zn1 position. The solvent cap was relaxed by means of energy minimization and 60 ps of molecular dynamics using the SANDER program[45] and the parm94 version of the all-atom AMBER force field.[46] Following the nonbonded approach, the metal ions were represented by charges (+2) and van der Waals parameters.[47,48] The resulting structure of the MMP-2 catalytic domain was employed as a template to dock the B3LYP/LACVP* cluster models of the active site.

QM/MM geometry optimizations were carried out using the version 5.5 of the Qsite program.[34,49] QM−MM interfaces were placed at the His_{403}@Cα−N, Phe_{405}@N−Cα, His_{407}@Cβ−Cα, and His_{413}@Cβ−Cα bonds.[34] In addition, the QM region included the catalytic Zn1 and the four water molecules closest to this metal ion. The QM region comprised a total of 67 QM atoms with a net charge of +1 and was described at the B3LYP/LACVP* level of theory (781 basis functions). The rest of the protein and solvent atoms were treated with the OPLS-AA force field. The Qsite methodology has been validated over a range of test cases, including relative conformational energies of dipeptides, deprotonation energies of amino acid side chains, and computations of binding energies and energies of transition states and intermediates for a number of enzymes, including metallo-enzymes such as hemerythrin,[50] cytochrome P450,[51] and methane monoxygenase.[35]

During QM/MM geometry optimizations, protein residues 10 Å beyond the catalytic zinc ion were frozen, whereas the position of those residues located at 8−10 Å from the zinc were harmonically restrained (force constant of 25 kcal/(Å^2 mol)). In addition, 35 water molecules close to the Zn1 site were optimized. Minimizations were performed without a nonbond cutoff until the root-mean-squared residual gradient was less than 5.0×10^{-4} in au, permitting thus a proper relaxation of the QM region and the proximal protein residues.

To remove the energetic noise produced by the differences in the MM energy contributions of the MM water molecules, as well as to include the effects of long-range electrostatic interactions by means of PB calculations, the coordinates of the MM water molecules in the optimized QM/MM structures were deleted after geometry optimization. Then single-point QM/MM calculations were carried out in order to estimate the

energy of the protein systems in the gas phase. Subsequently, the electrostatic contribution to the solvation free energy (ΔG^0_{solv}) for the different QM/MM optimized structures was determined within the PB approach using the Delphi program. The protein was represented as a low dielectric continuum (a value of $\epsilon_{int} = 1$ was used in the calculations) with embedded charges, and the solvent was represented as a high dielectric continuum ($\epsilon_{out} = 80$) with no salt. The OPLS-AA atomic charges were used for the protein atoms excepting those atoms that were within the QM region during QM/MM geometry optimizations. For these atoms, we used their ESP charges derived from single-point B3LYP/LACVP* calculations on the QM region of the corresponding QM/MM optimized geometries after having placed H-link atoms at the QM/MM cuts (a zero value to the atomic charges of the H-link atoms was assigned in the ESP fitting procedure using the RESP program, a part of the AMBER8 package).

Results

Validation Calculations. The relative energetic stability of the Zn1 configurations shown in Scheme 1 is governed by several factors: (1) the intrinsic basicity of the Zn1-bound water molecule and the Glu_{404} side chain, (2) the flexibility of the first coordination shell around Zn1, (3) the strength of the H-bond network interconnecting the important water molecules in the active site and the Glu_{404} side chain, and (4) long-range protein−protein and protein−solvent interactions. In principle, all of these energetic contributions can be taken into account by means of QM/MM calculations using the B3LYP/LACVP* QM level of theory. However, to better calibrate the performance of the B3LYP/LACVP* level as applied to our particular problem, we optimized in the gas phase a series of small model compounds at the B3LYP/LACVP* and the ab initio MP2/6-31+G** levels of theory.

The series of small compounds that were considered for validation purposes comprises van der Waals complexes (e.g., $[Zn(OH)]^+\cdots H_2O$, $[Zn-(OH)]^+\cdots(HOOC-CH_3)$, etc.) as well as zinc complexes with various coordination numbers (e.g., a tetrahedral $[Zn(NH_3)_3(H_2O)]^{2+}(H_2O)_2$ complex, a bipyramidal $[Zn(NH_3)_3(H_2O)_2]^{2+}(H_2O)$ structure, etc.). All of the optimized geometries are reported in Figure S1 of Supporting Information. From these calculations, we found that the mean unsigned difference (MUD) in the Zn···O bond lengths between B3LYP/LACVP* and MP2/6-31+G** amounts to 0.075 Å. The largest discrepancy arises in the Zn···O (apical water) distance of the bipryamidal model complexes for which B3LYP/LACVP* gives values close to 2.2 Å, 0.2 Å shorter than the MP2/6-31+G** ones. In terms of the O···H distances of hydrogen bond interactions, the corresponding MUD is 0.065 Å. Taking into account these moderate differences in the important bond lengths and the fact that both B3LYP/LACVP* and MP2/6-31+G** predict the same trends in the change of the zinc−ligand distances upon rearrangement of the first shell ligands or deprotonation of the Zn-bound water, we conclude that B3LYP/LACVP* can yield reasonable structures for the large zinc complexes studied in this work.

From the absolute energies of the small model compounds, a set of 22 relative energies in the gas phase were derived including ligand rearrangement processes (e.g., TD $[Zn(NH_3)_3(H_2O)]^{2+}(H_2O)_2 \rightarrow$ HX $[Zn(NH_3)_3(H_2O)_3]^{2+}$; see the ΔE_{coord} values in Table 1), zinc−ligand bonding (e.g., $Zn^{2+}\cdots(OH_2)$), intermolecular interactions between the first and the second shell ligands (e.g., $[Zn(NH_3)_3(OH)]^+\cdots 2(H_2O)$, see the E_{int} data in Table 1), and proton exchange processes ($CH_3COO^- + [Zn(NH_3)_3(H_2O)]^{2+} \rightarrow [Zn(NH_3)_3(OH)]^+ + CH_3COOH$; ΔE_{rxnn} in Table 1). The MUD between the B3LYP/LACVP* relative energies in the gas phase and those obtained from composite CCSD(T) and MP2 energies was only 3.0 kcal/mol. The relative energies of the ligand rearrangement and the proton exchange processes were recomputed in an aqueous solution by adding the corresponding free energy solvation terms as estimated by SCRF PB calculations ($\epsilon_r = 80$). In the solution, the MUD between B3LYP/LACVP* and ab initio is 4.0 kcal/mol, a value which is still within reasonable bounds. Overall, we conclude that the B3LYP/LACVP* level can predict relative energies for the zinc complexes studied in this work within the general accuracy (3.0−5.0 kcal/mol) of the DFT methodologies.

QM Cluster Models. For the cluster model of the MMP-2 active site, a total of 13 critical points were located on the B3LYP/LACVP* PES (see Figure 1). All of these critical points correspond to energy minima on the PES according to analytical frequency calculations. Four-, five-, and six-coordinated forms of the catalytic Zn1 ion were investigated (see the **TD**, **BP**, and **HX** series of structures in Figure 1, respectively). In these structures, the Zn1 ion is bonded to three methyl-imidazole molecules and one to three water molecules. For each coordination mode of the Zn1 ion, two protonation states of the Zn1−water···Glu_{404} association were examined: (a) an ionic $[Zn-(OH_2)]^{2+}\cdots{}^-OOC$-$Glu_{404}$ contact and (b) a $[Zn-(OH)]^+\cdots$ HOOC-Glu_{404} hydrogen bond (see, e.g., the **TD**−**WAT** and **TD**−**OH** structures in Figure 1). Taking into account that the Glu_{404} residue was mutated into alanine in the original X-ray structure, the two Oϵ atoms of Glu_{404} were considered as proton acceptors, and different orientations of the Glu_{404} side chain were considered in the QM calculations (see **TD**−**WAT1** and **TD**−**WAT2**, etc.).

We see in Figure 1 that the Zn1−ligand bond distances increase with the coordination number of the zinc ion. The four-coordinated complexes (**TD**−**WAT** and **TD**−**OH**) present Zn−N and Zn−O bond lengths of 2.1 and 1.9−2.0 Å, respectively; meanwhile, these values change to 2.1−2.4 (Zn−N) and 2.0−2.2 Å (Zn−O) for the five-coordinated complexes (**BP**−**WAT** and **BP**−**OH**), and they range between 2.2 and 2.3 (Zn−N) and 2.0 and 2.4 Å (Zn−O) for the six-coordinated structures (**HX**−**WAT** and **HX**−**OH)**. In all of the complexes, the water/hydroxyl molecule bridging the Zn1 ion and the carboxylate/carboxylic group of Glu_{404} (W1 in Figure 1) presents the shortest Zn−O bond distance.

Concerning the overall coordination geometry of Zn1, we found that the four- and five-coordinated zinc complexes exhibit distorted tetrahedral and trigonal bipyramidal geometries, respectively. The His_{413}@Nϵ−Zn1−O@W1 bond angle, which has values around 130−140 and 145−160° in the **TD** and **BP** structures, respectively, shows the largest deviation from the reference values (109.4° and 120.0°). This effect can be traced to the influence of the Glu_{404} carboxylate/carboxylic group interacting with the water/hydroxide W1 molecule, reflecting, thus, the importance of the second shell Glu_{404} residue in modulating the coordination environment around the Zn1 ion. On the other hand, the six-coordinated complexes present a more regular octahedral arrangement around the metal ion with X−Zn1−Y angles close to 90°.

Table 2contains the gas-phase B3LYP/LACVP* electronic energies, the gas-phase thermal corrections to free energy, and the solvation free energies for the different QM structures.

In the gas phase, the five-coordinated cluster models (**BP**) are clearly favored with the nearly isoenergetic **BP**−**OH3** and **BP**−**WAT2** structures being the most stable ones. The gas-

TABLE 1: Ab Initio and DFT Energies (in kcal/mol) both in the Gas Phase and in Solution (Values in Italics) for Selected Ligand Rearrangements (ΔE_{coord}), Bonding Interactions (E_{int}), and Proton Exchange Processes (ΔE_{rxn}) Involving Small Compounds Relevant to the MMP-2 Active Site Configurations Examined in This Work[a]

	system	ab initio[b]		DFT[c]		difference[d]	
ΔE_{coord}	TD $[Zn(NH_3)_3(H_2O)]^{2+}(H_2O)_2 \rightarrow$ BP $[Zn(NH_3)_3(H_2O)_2]^{2+}(H_2O)$	−0.50	*−0.30*	−4.76	*−4.03*	4.27	*3.73*
ΔE_{coord}	TD $[Zn(NH_3)_3(H_2O)]^{2+}(H_2O)_2 \rightarrow$ HX $[Zn(NH_3)_3(H_2O)_3]^{2+}$	7.16	*4.35*	5.35	*1.75*	1.81	*2.60*
ΔE_{coord}	TD $[Zn(NH_3)_3(OH)]^{+}(H_2O)_2 \rightarrow$ BP $[Zn(NH_3)_3(OH)(H_2O)]^{+}(H_2O)$	−4.50	*9.96*	−8.90	*5.28*	4.40	*4.68*
ΔE_{coord}	TD $[Zn(NH_3)_3(OH)]^{+}(H_2O)_2 \rightarrow$ HX $[Zn(NH_3)_3(OH)(H_2O)_2]^{+}$	−14.42	*6.37*	−19.26	*−1.96*	4.84	*8.33*
ΔE_{coord}	TD $[Zn(NH_3)_3(H_2O)]^{2+}(H_2O) \rightarrow$ BP $[Zn(NH_3)_3(H_2O)_2]^{2+}$	4.83	*2.89*	3.28	*0.84*	1.55	*2.06*
ΔE_{coord}	TD $[Zn(NH_3)_3(OH)]^{+}(H_2O) \rightarrow$ BP $[Zn(NH_3)_3(OH)(H_2O)]^{+}$	−0.42	*14.04*	−4.24	*8.56*	3.82	*5.48*
E_{int}	$(H_2O)\cdots(H_2O)$	−4.43		−5.53		1.10	
E_{int}	$(OH)^{-}\cdots(H_2O)$	−19.50		−22.47		2.97	
E_{int}	$Zn^{2+}\cdots(OH)^{-}$	−424.93		−428.45		3.52	
E_{int}	$Zn^{2+}\cdots(OH_2)$	−96.05		−97.17		1.12	
E_{int}	$[Zn-(OH)]^{+}\cdots(H_2O)$	−14.07		−17.45		3.38	
E_{int}	$[Zn-(OH)]^{+}\cdots(HOOC-CH_3)$	−17.83		−18.79		0.96	
E_{int}	$[Zn(NH_3)_3(H_2O)_2]^{2+}\cdots(H_2O)$	−29.74		−31.60		1.86	
E_{int}	$[Zn(NH_3)_3(OH)(H_2O)]^{+}\cdots(H_2O)$	−13.98		−15.87		1.89	
E_{int}	$[Zn(NH_3)_3(H_2O)]^{2+}\cdots 2(H_2O)$	−47.82		−50.68		2.86	
E_{int}	$[Zn(NH_3)_3(OH)]^{+}\cdots 2(H_2O)$	−13.97		−14.70		0.73	
ΔE_{rxn}	$CH_3COO^{-} + [Zn(NH_3)_3(H_2O)]^{2+}(H_2O)_2 \rightarrow [Zn(NH_3)_3(OH)]^{+}(H_2O)_2 + CH_3COOH$	−170.31	*4.94*	−173.42	*3.21*	3.11	*1.73*
ΔE_{rxn}	$CH_3COO^{-} + [Zn(NH_3)_3(H_2O)_2]^{2+}(H_2O) \rightarrow [Zn(NH_3)_3(OH)(H_2O)]^{+}(H_2O) + CH_3COOH$	−174.31	*15.21*	−177.55	*12.52*	3.24	*2.68*
ΔE_{rxn}	$CH_3COO^{-} + [Zn(NH_3)_3(H_2O)_3]^{2+} \rightarrow [Zn(NH_3)_3(OH)(H_2O)_2]^{+} + CH_3COOH$	−191.89	*6.96*	−198.03	*−0.50*	6.14	*7.46*
ΔE_{rxn}	$CH_3COO^{-} + [Zn(NH_3)_3(H_2O)]^{2+}(H_2O) \rightarrow [Zn(NH_3)_3(OH)]^{+}(H_2O) + CH_3COOH$	−182.41	*0.99*	−184.75	*0.87*	2.35	*0.11*
ΔE_{rxn}	$CH_3COO^{-} + [Zn(NH_3)_3(H_2O)_2]^{2+} \rightarrow [Zn(NH_3)_3(OH)(H_2O)]^{+} + CH_3COOH$	−187.65	*12.13*	−192.27	*8.60*	4.62	*3.54*
ΔE_{rxn}	$CH_3COO^{-} + [Zn(NH_3)_3(H_2O)]^{2+} \rightarrow [Zn(NH_3)_3(OH)]^{+} + CH_3COOH$	−197.71	*1.31*	−203.30	*−5.42*	5.59	*6.73*

[a] All of the zinc complexes were optimized imposing C_s symmetry constraints. Interaction energies (E_{int}) were computed by means of the counterpoise method in order to minimize the basis set superposition error. [b] Using an additive combination of electronic energies (CCSD(T)/6-31+G** + MP2/6-311+G(3df,2p) − MP2/6-31+G**). Ab initio energies in solution include the free solvation energy computed at the HF/6-31+G** level of theory. [c] B3LYP/LACVP* electronic energies. Values in solution include the B3LYP/LACVP* free solvation energy. [d] Ab initio − DFT unsigned energy difference. The average value of this unsigned energy difference is 3.00 kcal/mol.

phase energies also show that the tetrahedral coordination is intrinsically disfavored (>10 kcal/mol) with respect to the five- and six-coordinated forms. A first approximation to the environment effects was obtained by means of SCRF calculations using three different values for the dielectric constant of the surrounding continuum ($\epsilon = 80$, 20, and 4). Regardless of the ϵ value, it turns out that the polarizable continuum stabilizes by around 8−10 kcal/mol for the four-coordinated clusters with respect to the five- and six-coordinated ones. The free energies in aqueous solution (ΔG) can be estimated by adding the relative ΔG_{solv} values ($\epsilon = 80$) to the gas-phase B3LYP energies and by adding the thermal corrections to the free energy. In this way, all of the QM structures become close to each other in terms of their ΔG values (see Table 2). The **TD−OH1**, **BP−OH3**, and **BP−WAT2** complexes become the most stable structures in solution, although other coordination modes such as the octahedral complex **HX−WAT** are only around 2−4 kcal/mol less stable.

As mentioned in Methods, solvation energies for the QM cluster models were also computed with the Delphi program using $\epsilon = 80$. The Delphi calculations use a fixed charge distribution (B3LYP/LACVP* ESP charges) for the solute atoms, which neglect polarization effects. Nevertheless, comparison of the QM SCRF and Delphi ΔG_{solv} values shows that Delphi predicts *relative* solvation energies ($\Delta\Delta G_{solv}$) quite similar to the QM SCRF ones, the average and maximum energy differences being 1.4 and 3.1 kcal/mol, respectively. These moderate differences in the relative solvation energies validate the use of the Delphi electrostatic calculations to estimate solvation effects on the QM/MM optimized structures of the MMP-2 catalytic domain (see below).

QM/MM Calculations on the MMP-2 Catalytic Domain. To further evaluate the effect of the protein and solvent environment on the coordination of the catalytic zinc ion, we performed QM/MM energy minimizations of different Zn1 complexes within the catalytic domain of the MMP-2 enzyme followed by PB calculations. The optimized QM/MM structures are displayed in Figure 2 while their energies are collected in Table 3.

The QM/MM energy minimizations of the enzyme models were started at geometries obtained by rigid docking of the 13 QM cluster models into the MMP-2 active site. After energy minimizations, we obtained a series of nine QM/MM structures in which the Zn1 ion is again coordinated in tetrahedral (**TD**), trigonal bipyramidal (**BP**), or octahedral arrangements (**HX**). With respect to the QM cluster models, the Zn1 environment shows slight conformational differences affecting mainly the water molecules and the Glu_{404} side chain in the QM region (see Figures 1 and 2). Thus, the Zn−L QM/MM bond distances were comparable to the QM ones, the W1 molecule exhibits

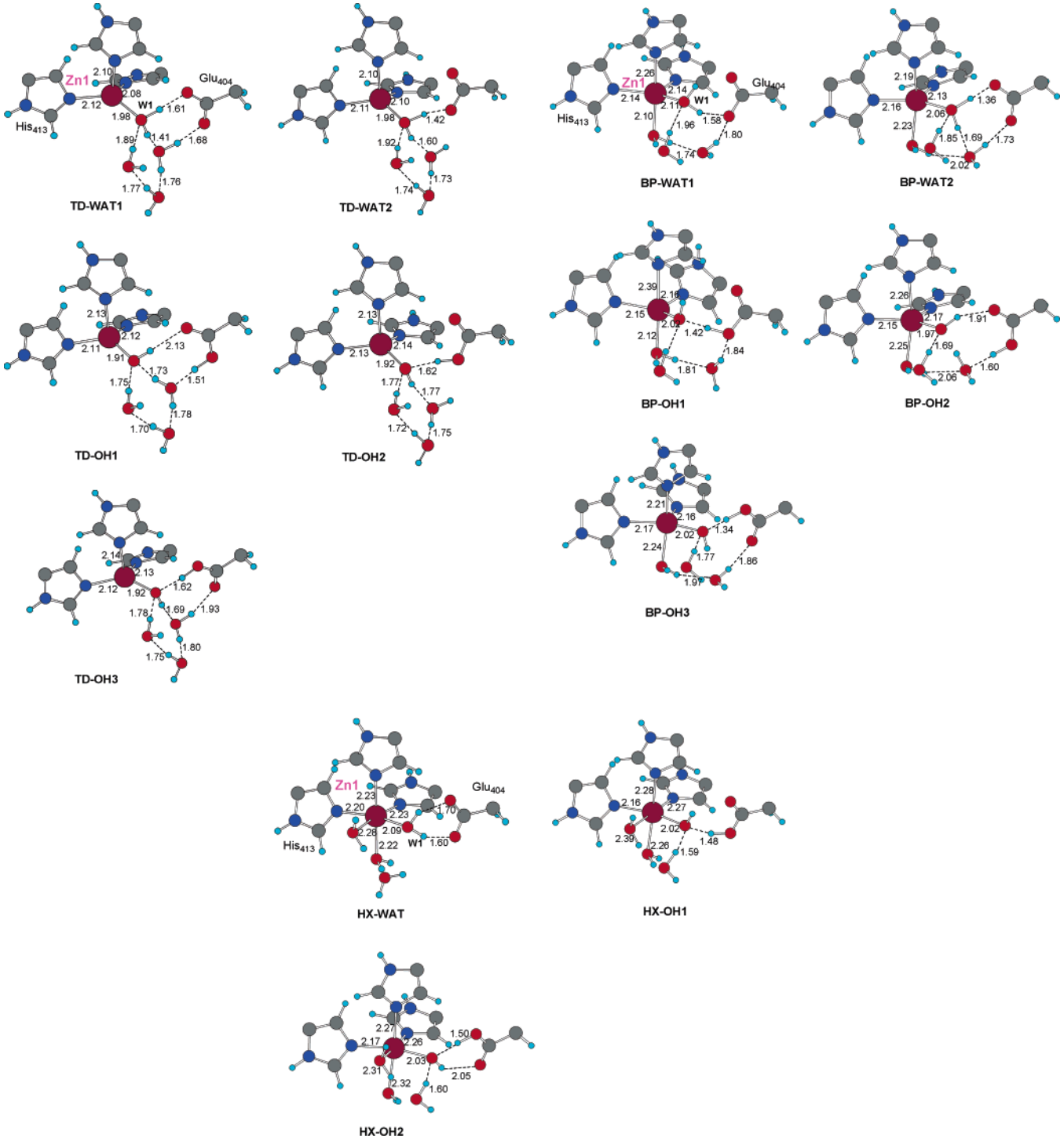

Figure 1. Optimized structures obtained for the four-, five-, and six-coordinated cluster model of the MMP-2 active site. For the sake of clarity, the modeled β4 strand and the fixed methylene groups are not represented. Distances are in Å.

again the shortest Zn−L QM/MM distance, the L−Zn−L QM/MM bond angles are slightly deviated from the reference values, and so forth (see Table S2, Supporting Information). The most important structural difference between the QM/MM and the QM results is the absence of a **HX−OH** configuration among the QM/MM optimized structures (i.e., Zn1 coordinated to three imidazole rings, two water molecules, and one hydroxide anion (W1)). In fact, only one QM/MM structure with six coordination (**HX−WAT)** was found. In contrast, the four- and five-coordinated QM/MM complexes exhibit either a $[Zn-(OH_2)]^{2+}\cdots{}^{-}OOC-Glu_{404}$ salt bridge (**BP−WAT1**, **BP−WAT2**, and **TD−WAT**) or a $[Zn-(OH)]^{+}\cdots HOOC-Glu_{404}$ H-bond (**BP−OH1**, **BP−OH2**, **TD−OH1**, **TD−OH2**, and **TD−OH3**) in several conformations.

As mentioned in Methods, the MM water molecules were removed from the optimized QM/MM structures in order to carry out single-point QM/MM and Delphi calculations. The resulting QM/MM and ΔG_{solv} energies are collected in Table 3 for the different structures. Similarly to the QM energies computed for the cluster models, the QM/MM energies of the five-coordinated complexes are lower than those of the tetrahedral ones. A closer view of the QM/MM energies shows that the protein environment tends to stabilize the salt bridge $[Zn-(OH_2)]^{2+}\cdots{}^{-}OOC-Glu_{404}$ interaction since the QM/MM energy

TABLE 2: Total Energies (au), Thermal Corrections to Gibbs Free Energies (au), and Solvation Energies (kcal/mol) Obtained for the Cluster Models of the MMP-2 Active Site[a]

			ΔG_{solv}[c]				
			SCRF			Delphi	
	B3LYP/LACVP*	G_{therm}[b]	$\epsilon = 80$	$\epsilon = 20$	$\epsilon = 4$	$\epsilon = 80$	ΔG[d]
TD−WAT1	−2178.820244	0.561516	−85.50	−81.51	−60.21	−79.02	0.0
	(0.0)	(0.0)	(0.0)	(0.0)	(0.0)	(0.0)	
TD−WAT2	−2178.818871	0.560518	−82.92	−78.73	−58.34	−75.95	2.9
	(0.9)	(−0.6)	(2.6)	(2.8)	(1.9)	(3.1)	
TD−OH1	−2178.829984	0.562711	−84.32	−79.95	−58.98	−75.63	−4.1
	(−6.1)	(0.8)	(1.2)	(1.6)	(1.2)	(3.4)	
TD−OH2	−2178.825392	0.561797	−82.13	−77.95	−57.76	−75.00	0.4
	(−3.2)	(0.2)	(3.4)	(3.6)	(2.4)	(4.0)	
TD−OH3	−2178.823443	0.563823	−81.73	−77.94	−58.18	−76.06	3.2
	(−2.0)	(1.4)	(3.8)	(3.6)	(2.0)	(3.0)	
BP−WAT1	−2178.838847	0.561268	−73.69	−70.06	−52.24	−67.18	−0.1
	(−11.7)	(−0.2)	(11.8)	(11.4)	(8.0)	(11.8)	
BP−WAT2	−2178.844846	0.563638	−73.71	−69.87	−51.60	−65.93	−2.3
	(−15.4)	(1.3)	(11.8)	(11.6)	(8.6)	(13.1)	
BP−OH1	−2178.839341	0.560664	−72.90	−69.26	−51.18	−64.76	0.1
	(−12.0)	(−0.5)	(12.6)	(12.2)	(9.0)	(14.3)	
BP−OH2	−2178.840743	0.563604	−72.04	−68.31	−50.53	−64.01	1.9
	(−12.9)	(1.3)	(13.5)	(13.2)	(9.7)	(15.0)	
BP−OH3	−2178.846201	0.563437	−73.29	−69.58	−51.55	−65.77	−2.9
	(−16.3)	(1.2)	(12.2)	(11.9)	(8.7)	(13.2)	
HX−WAT	−2178.835994	0.561589	−75.54	−71.62	−52.90	−65.93	0.1
	(−9.9)	(0.0)	(10.0)	(9.9)	(7.3)	(13.1)	
HX−OH1	−2178.838605	0.561979	−71.46	−67.74	−50.06	−63.01	2.8
	(−11.5)	(0.3)	(14.0)	(13.8)	(10.2)	(16.0)	
HX−OH2	−2178.835863	0.562582	−72.74	−68.92	−50.82	−63.89	3.7
	(−9.8)	(0.7)	(12.8)	(12.6)	(9.4)	(15.1)	

[a] Relative energies (kcal/mol) are included in parentheses. [b] From B3LYP/LACVP* analytical frequencies. [c] Single-point calculations on the B3LYP/LACVP* geometries. [d] $\Delta G \approx \Delta E_{QM} + \Delta G_{therm} + \Delta\Delta G_{solv}$ (SCRF, $\epsilon = 80$).

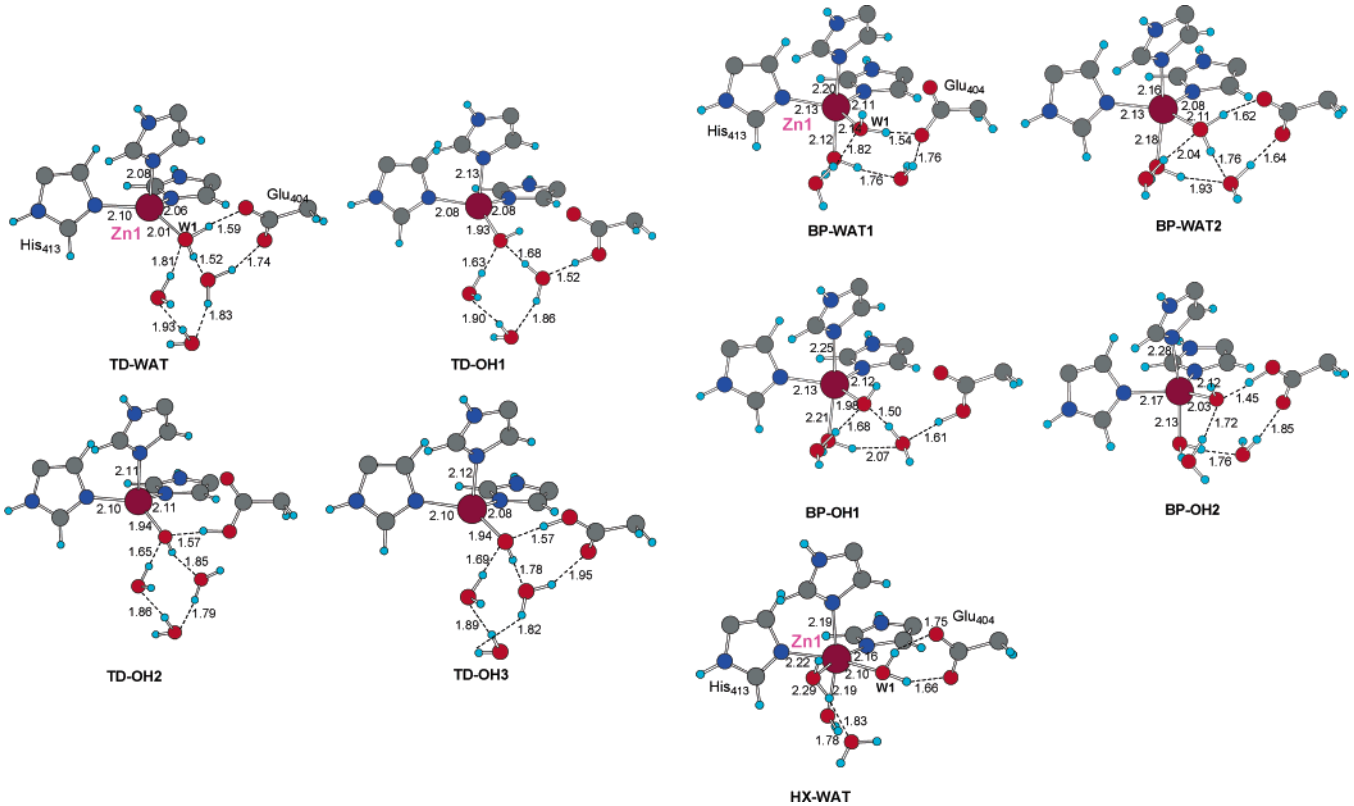

Figure 2. Coordination spheres around the catalytic zinc ion as extracted from the QM/MM optimized structures of the MMP-2 catalytic domain. Distances are in Å.

of the **BP−WAT2** complex is around 2 kcal/mol more stable than those of **BP−OH1** and **BP−OH2**. Inclusion of solvent effects by adding the ΔG_{solv} energies to the relative QM/MM energies reinforces slightly the energetic preference for **BP−WAT2**, which remains the most stable configuration in terms of the approximate free energy in the enzyme (see Table 3). However, the free energy of **BP−WAT2** is only 2.2, 2.4, and 2.7 kcal/mol lower than those of the **BP−OH1**, **TD−OH1**, and

TABLE 3: Total QM/MM Energies (au) and Solvation Energies (ΔG_{solv} in kcal/mol) Obtained for Different Zn1 Complexes in the Catalytic Domain of MMP-2[a]

	$E_{QM/MM}$[b]	ΔG_{solv}[c] ($\epsilon = 80$)	ΔG[d]
TD−WAT1	−1844.46913 (0.0)	−2191.4 (0.0)	0.0
TD−OH1	−1844.47708 (−5.0)	−2194.7 (−3.3)	−8.3
TD−OH2	−1844.47299 (−2.4)	−2185.8 (5.6)	3.2
TD−OH3	−1844.47269 (−2.2)	−2190.7 (0.7)	−1.5
BP−WAT1	−1844.47890 (−6.1)	−2191.0 (0.4)	−5.7
BP−WAT2	−1844.48177 (−7.9)	−2194.1 (−2.7)	−10.6
BP−OH1	−1844.47801 (−5.6)	−2194.3 (−2.9)	−8.5
BP−OH2	−1844.47910 (−6.2)	−2190.8 (0.6)	−5.6
HX−WAT	−1844.47862 (−6.0)	−2193.4 (−2.0)	−8.0

[a] Relative QM/MM and ΔG_{solv} energies (kcal/mol) are included in parentheses, and relative free energies (ΔG in kcal/mol) are also shown. [b] B3LYP/LACVP*//OPLS-AA. [c] Computed with Delphi using OPLS-AA and QM ESP atomic charges. [d] $\Delta G \approx \Delta E_{QM/MM} + \Delta\Delta G_{solv}$.

HX−WAT structures, respectively. Since these energy differences are small, the four structures (**BP−WAT2**, **BP−OH1**, **TD−OH1**, and **HX−WAT**) can be grouped together as the most likely configurations of the MMP-2 active site according to the QM/MM and PB calculations. The rest of the QM/MM structures (e.g., **TD−WAT1**, **TD−OH2**, etc.) are predicted to be much less stable by several kcal/mol.

It can be interesting to note that the QM/MM and PB calculations discriminate more sharply among the possible Zn1 configurations than the QM calculations do on the cluster models. The eight most stable QM cluster models have relative free energies within a 4 kcal/mol range while the enzyme calculations predict more accentuated energy differences, and only four QM/MM complexes lie in the lower end of the free energy range. Overall, the QM/MM and PB calculations predict a moderately flexible first coordination shell for the Zn1 ion, which could adopt the **BP−WAT2**, **BP−OH1**, **TD−OH1**, and **HX−WAT** arrangements. Other Zn1 coordination modes can be discarded on the basis of the QM/MM calculations (tetrahedral coordination arises only when the Zn1 ion is bound to a hydroxide anion, six coordination implies only water molecules, etc.).

Discussion

Coordination of the Catalytic Zinc Ion in the Active Form of MMPs. The conserved zinc binding motif in MMPs, HEXXHXXGXXH, is characterized by short spacers between the zinc binding residues which would suggest a rather rigid coordination shell around the catalytic zinc ion.[52] However, as mentioned in Introduction, the crystallographic analyses have revealed that the Zn1 ion in the catalytic domain of the MMPs can have a coordination number of four, five, or six depending on the nature of the surrounding ligands. More particularly, the X-ray structures show that Zn1 can bind to one to three water molecules in addition to the three conserved histidine residues.

To increase our knowledge about the relative stability and geometrical details of the possible Zn1 coordination environments and the protonation state of the important water molecules and Glu_{404}, we characterized in this work a family of zinc complexes, relevant to the MMP active site, presenting four, five, or six coordination using QM calculations on cluster models and QM/MM and PB calculations on the catalytic domain of the MMP-2 enzyme. The QM/MM and PB calculations predict that the most stable configuration in the MMP-2 active enzyme presents a catalytic zinc ion coordinated by the three conserved histidines and two water molecules in a slightly distorted trigonal bipyramidal arrangement (**BP−WAT2** in Figure 2). In this structure, one water molecule (W1) bridges the Zn1 ion and the carboxylate group of the catalytically relevant Glu_{404} residue, which could activate the Zn1-bound water molecule during the hydrolysis of peptide substrates. The second water molecule bound to Zn1 points toward bulk solvent and could be easily displaced by the carbonyl group of the scissile peptide bond during substrate binding. In good agreement with the observations from the X-ray studies of MMPs, the QM/MM calculations predict that the local structure of the MMP-2 catalytic site can easily adopt various coordination environments around the catalytic zinc ion, given that the **BP−WAT2** configuration has a very similar stability to the six-coordinated structure **HX−WAT**, the five-coordinated model **BP−OH1** with a Zn1-bound hydroxide, and the tetrahedral **TD−OH1** complex. The energy differences among these structures are smaller (<2.4 kcal/mol) than the typical accuracy of DFT methodologies.

From a methodological point of view, it may be interesting to note that the structures obtained from the QM calculations on the active site cluster model are quite similar to those resulting from the QM/MM calculations on the solvated catalytic domain. In terms of relative free energies, however, the QM free energies of the cluster models should be treated with caution given that protein environments are not homogeneous media characterized by a single dielectric constant. A more realistic description is provided by the QM/MM energies complemented with the PB solvation energies, which altogether include the effects of the protein residues and solvent.

Mechanistic Implications. Interestingly, the four most stable Zn1 complexes predicted by our calculations could all be catalytically relevant. Most likely, the pre-reactive MMP complexes formed with peptide substrates would exhibit the distorted trigonal bipyramidal arrangement around Zn1 in which the carbonyl group of the scissile bond would be the fifth ligand. The five-coordination mode can also be favorable for catalysis because it shows two charge configurations, **BP−WAT2** and **BP−OH1**, which are nearly isoenergetic. On the other hand, four-coordinated structures can appear in the peptide hydrolysis process as shown by previous QM/MM calculations on a cluster model of the MMP-3 active site.[53] According to these calculations, the rate determining transition structure has a forming C@peptide···O@W1 distance of 1.59 Å, and Zn1···O@W1 and Zn1···O@pep distances of 2.54 and 1.97 Å, respectively, while the Glu_{404} side chain is neutral. Finally, six-coordination could be present in the product complex formed after the hydrolysis reaction as suggested by the X-ray structure of the F171D mutant of the catalytic domain of MMP-12, which presents two additional N-terminal methionine residues and a Zn1 ion coordinated by three water molecules in an octahedral fashion.[21] In this X-ray structure, the arrangement of the N-terminal NH_3^+ group could correspond to that of the amine product formed after the hydrolysis of a peptide substrate.

Acknowledgment. This research was supported by the Spanish MEC via the Ramon y Cajal program and Grant CTQ2004-06309. The allocation of computer time at the

CIEMAT and at the Centro Nacional de Supercomputación (Barcelona Supercomputer Center) is also acknowledged.

Supporting Information Available: Figures S1−S3, Tables S1 and S2, and ZIP files containing the QM/MM optimized models of the MMP-2 catalytic domain. This material is available free of charge via the Internet at http://pubs.acs.org.

References and Notes

(1) McCawley, L. J.; Matrisian, L. *Curr. Opin. Cell Biol.* **2001**, *13*, 534.
(2) Lee, M.-H.; Murphy, G. *J. Cell Sci.* **2004**, *117*, 4015.
(3) Werb, Z. *Cell* **1997**, *91*, 439.
(4) Sternlicht, M. D.; Werb, Z. *Annu. Rev. Cell Dev. Biol.* **2001**, *17*, 463.
(5) Egeblad, M.; Werb, Z. *Nat. Rev. Cancer* **2002**, *2*, 163.
(6) Fingleton, B. *Front. Biosci.* **2006**, *11*, 479.
(7) Van Meurs, J.; van Lent, P.; Holthuysen, A.; Lambrou, D.; Bayne, E.; Singer, I.; van den Berg, W. *J. Immunol.* **1999**, *163*, 5633.
(8) Burrage, P. S.; Mix, K. S.; Brinckerhoff, C. E. *Front. Biosci.* **2006**, *11*, 529.
(9) Whittaker, M.; Floyd, C. D.; Brown, P.; Gearing, A. J. H. *Chem. Rev.* **1999**, *99*, 2735.
(10) Bigg, H. F.; Rowan, A. D. *Curr. Opin. Pharmacol.* **2001**, *1*, 314.
(11) Hoekstra, R.; Eskens, F. A. L. M.; Verweij, J. *Oncologist* **2001**, *6*, 415.
(12) Mannello, F.; Tonti, G.; Papa, S. *Curr. Cancer Drug Targets* **2005**, *5*, 285.
(13) Bode, W.; Fernandez-Catalan, C.; Tschesche, H.; Grams, F.; Nagase, H.; Maskos, K. *Cell. Mol. Life Sci.* **1999**, *55*, 639.
(14) Nagase, H.; Woessner, J. F., Jr. *J. Biol. Chem.* **1999**, *274*, 21491.
(15) Bertini, I.; Calderone, V.; Cosenza, M.; Fragai, M.; Lee, Y.-M.; Luchinat, C.; Mangani, S.; Terni, B.; Turano, P. *Proc. Natl. Acad. Sci. U.S.A.* **2005**, *102*, 5334.
(16) Maskos, K. *Biochimie* **2005**, *87*, 249.
(17) Johnson, L. L.; Pavlovsky, A. G.; Johnson, A. R.; Janowick, J. A.; Man, C.-F.; Ortwine, D. F.; Purchase, C. F., II; White, A. D.; Hupe, D. J. *J. Biol. Chem.* **2000**, *275*, 11026.
(18) Arza, B.; De Maeyer, M.; Félez, J.; Collen, D.; Lijnen, H. R. *Eur. J. Biochem.* **2001**, *268*, 826.
(19) Chen, L.; Rydel, T. J.; Gu, F.; Dunaway, C. M.; Pikul, S.; McDow Dunham, K.; Barnett, B. L. *J. Mol. Biol.* **1999**, *293*, 545.
(20) Engel, C. K.; Pirard, B.; Schimanski, S.; Kirsch, R.; Habermann, J.; Klingler, O.; Schlotte, V.; Weithmann, K. U.; Wendt, K. U. *Chem. Biol.* **2005**, *12*, 181.
(21) Bertini, I.; Calderone, V.; Fragai, M.; Luchinat, C.; Mangani, S.; Terni, B. *Angew. Chem., Int. Ed.* **2003**, *42*, 2673.
(22) Kleifeld, O.; Van den Steen, P. E.; Frenkeli, A.; Cheng, F.; Jiang, H. L.; Opdenakker, G.; Sagi, I. *J. Biol. Chem.* **2000**, *275*, 34335.
(23) Kleifeld, O.; Kotra, L. P.; Gervasi, D. C.; Brown, S.; Bernardo, M. M.; Fridman, R.; Mobashery, S.; Sagi, I. *J. Biol. Chem.* **2001**, *276*, 17125.
(24) Morgunova, E.; Tuuttila, A.; Bergmann, U.; Isupov, M.; Lindqvist, Y.; Schneider, G.; Tryggvason, K. *Science* **1999**, *284*, 1667.
(25) Jozic, D.; Bourenkov, G.; Lim, N.-H.; Visse, R.; Nagase, H.; Bode, W.; Maskos, K. *J. Biol. Chem.* **2005**, *280*, 9578.
(26) Gomis-Rüth, F.-X.; Maskos, K.; Betz, M.; Bergner, A.; Huber, R.; Suzuki, K.; Yoshida, N.; Nagase, H.; Brew, K.; Bourenkovk, G. P.; Bartunikk, H.; Bode, W. *Nature* **1997**, *389*, 77.
(27) Fernandez-Catalan, C.; Bode, W.; Huber, R.; Turk, D.; Calvete, J. J.; Lichte, A.; Tschesche, H.; Maskos, K. *EMBO J.* **1998**, *17*, 5238.
(28) Browner, M. F.; Smith, W. W.; Castelhano, A. L. *Biochemistry* **1995**, *34*, 6602.
(29) Gao, J.; Ma, S.; Major, D. T.; Nam, K.; Pu, J.; Truhlar, D. G. *Chem. Rev.* **2006**, *106*, 3188.
(30) Foda, H. D.; Zucker, S. *Drug Discovery Today* **2001**, *6*, 478.
(31) Becke, A. D. *J. Chem. Phys.* **1993**, *98*, 5648.
(32) Becke, A. D. Exchange-Correlation Approximation in Density-Functional Theory. In *Modern Electronic Structure Theory Part II*; Yarkony, D. R., Ed.; World Scientific: Singapore, 1995.
(33) Hay, P. J.; Wadt, W. R. *J. Chem. Phys.* **1985**, *82*, 299.
(34) Murphy, R. B.; Philipp, D. M.; Friesner, R. A. *J. Comput. Chem.* **2000**, *21*, 1442.
(35) Gherman, B. F.; Lippard, S. P.; Friesner, R. A. *J. Am. Chem. Soc.* **2004**, *127*, 1025.
(36) Siegbahn, P. E. M. *Q. Rev. Biophys.* **2003**, *36*, 91.
(37) Rasolov, V. A.; Pople, J. A.; Patner, M. A.; Windus, T. L. *J. Chem. Phys.* **1998**, *109*, 1223.
(38) Frisch, M. J.; Trucks, G. W.; Schlegel, H. B.; Scuseria, G. E.; Robb, M. A.; Cheeseman, J. R.; Montgomery, J. A., Jr.; Vreven, T.; Kudin, K. N.; Burant, J. C.; Millam, J. M.; Iyengar, S. S.; Tomasi, J.; Barone, V.; Mennucci, B.; Cossi, M.; Scalmani, G.; Rega, N.; Petersson, G. A.; Nakatsuji, H.; Hada, M.; Ehara, M.; Toyota, K.; Fukuda, R.; Hasegawa, J.; Ishida, M.; Nakajima, T.; Honda, Y.; Kitao, O.; Nakai, H.; Klene, M.; Li, X.; Knox, J. E.; Hratchian, H. P.; Cross, J. B.; Bakken, V.; Adamo, C.; Jaramillo, J.; Gomperts, R.; Stratmann, R. E.; Yazyev, O.; Austin, A. J.; Cammi, R.; Pomelli, C.; Ochterski, J. W.; Ayala, P. Y.; Morokuma, K.; Voth, G. A.; Salvador, P.; Dannenberg, J. J.; Zakrzewski, V. G.; Dapprich, S.; Daniels, A. D.; Strain, M. C.; Farkas, O.; Malick, D. K.; Rabuck, A. D.; Raghavachari, K.; Foresman, J. B.; Ortiz, J. V.; Cui, Q.; Baboul, A. G.; Clifford, S.; Cioslowski, J.; Stefanov, B. B.; Liu, G.; Liashenko, A.; Piskorz, P.; Komaromi, I.; Martin, R. L.; Fox, D. J.; Keith, T.; Al-Laham, M. A.; Peng, C. Y.; Nanayakkara, A.; Challacombe, M.; Gill, P. M. W.; Johnson, B.; Chen, W.; Wong, M. W.; Gonzalez, C.; Pople, J. A. *Gaussian 03*, revision C.02; Gaussian, Inc.: Wallingford, CT, 2004.
(39) Tannor, D. J.; Marten, B.; Murphy, R.; Friesner, R. A.; Sitkoff, D.; Nicholls, A.; Ringnalda, M.; Goddard, I. W. A.; Honig, B. *J. Am. Chem. Soc.* **1994**, *116*, 11875.
(40) *JAGUAR*, 5.5 ed.; Schrödinger, LLC: Portland, OR, 1991−2003.
(41) Rocchia, W.; Alexov, E.; Honig, B. *J. Phys. Chem. B* **2001**, *105*, 6507.
(42) Rocchia, W.; Sridharan, S.; Nicholls, A.; Alexov, E.; Chiabrera, A.; Honig, B. *J. Comput. Chem.* **2002**, *23*, 128.
(43) Massova, I.; Kotra, L. P.; Fridman, R.; Mobashery, S. *FASEB J.* **1998**, *12*, 1075.
(44) Dhanaraj, V.; Williams, M. G.; Ye, Q.-Z.; Molina, F.; Johnson, L. L.; Ortwine, D. F.; Pavlovsky, A.; Rubin, J. R.; Skeean, R. W.; White, A. D.; Humblet, C.; Hupe, D. J.; Blundell, T. L. *Croat. Chem. Acta* **1999**, *72*.
(45) Case, D. A.; Darden, T. A.; Cheatham, T. E. I.; Simmerling, C. L.; Wang, J.; Duke, R. E.; Luo, R.; Merz, K. M.; Wang, B.; Pearlman, D. A.; Crowley, M.; Brozell, S.; Tsui, V.; Gohlke, H.; Mongan, J.; Hornak, V.; Cui, G.; Beroza, P.; Schafmeister, C.; Caldwell, J. W.; Ross, W. S.; Kollman, P. A. *AMBER* 8, 8.0 ed.; University of California: San Francisco, CA, 2004.
(46) Cornell, W. D.; Cieplak, P.; Bayly, C. I.; Gould, I. R.; Merz, K. M., Jr.; Ferguson, D. M.; Spellmeyer, D. C.; Fox, T.; Caldwell, J. W.; Kollman, P. A. *J. Am. Chem. Soc.* **1995**, *117*, 5179.
(47) Aqvist, J. *J. Phys. Chem.* **1990**, *94*, 8021.
(48) Stote, R. H.; Karplus, M. *Proteins: Struct., Funct., Genet.* **1995**, *23*, 12.
(49) *Qsite*; Schrodinger, Inc.: Portland, OR, 2000.
(50) Wirstam, M.; Lippard, S. J.; Friesner, R. A. *J. Am. Chem. Soc.* **2003**, *125*, 3980.
(51) Guallar, V.; Friesner, R. A. *J. Am. Chem. Soc.* **2004**, *126*, 8501.
(52) Vallee, B. L.; Auld, D. S. *Proc. Natl. Acad. Sci. U.S.A.* **1990**, *87*, 220.
(53) Pelmenschikov, V.; Siegbahn, P. E. M. *Inorg. Chem.* **2002**, *41*, 5659.